Relationships Among Some Conservative Discretization Methods

THOMAS F. RUSSELL

Abstract

Relationships among various mass-conservative discretization techniques for equations of the type $-\nabla \cdot \mathbf{K}\nabla p = q$ on distorted logically rectangular meshes are discussed. The case of heterogeneous, anisotropic $\mathbf{K}$ is important for applications to subsurface porous media, in particular the groundwater flow equation and the pressure equation of petroleum reservoir simulation. Some methods are based on $\mathbf{K}$ itself, others on $\mathbf{K}^{-1}$. Within one of these groups, mass lumping and quadrature can be keys to understanding connections between methods; incomplete inversion of the mass matrix is useful in relating one group to the other.

KEYWORDS: conservation, distorted grid, finite volume, mixed method

1 Introduction

The purpose of this paper is to introduce some concepts that could be useful in understanding relationships among various types of conservative discretization methods. We concern ourselves particularly with finite volume, flux-based finite difference, and mixed finite element methods designed to calculate accurate fluxes on distorted meshes for problems with heterogeneous, anisotropic conductivity. Such procedures can be important in a variety of applications, particularly subsurface flows in porous media.

This study is merely introductory, and is far from exhaustive or definitive. The methods discussed here are sufficiently varied and complex that a complete analysis of their relationships would constitute a much longer paper. It is not our goal here to compare the merits of these approaches; other forums

Lecture Notes in Physics
Chen, Ewing, and Shi (eds.), pp. 1–16.

put here ISBN

will be more appropriate for that. We also do not address the nontrivial issues of solving the discrete equations arising from these methods. Rather, we seek some simple tools that can assist efforts to comprehend a "big picture" of discretizations that can fairly be described as confusing.

For simplicity of exposition, the spatial domain will be limited to 2-D, with 3-D mentioned only in passing. This is a significant simplification, because, for example, the edges of a quadrilateral (bilinear image of a square) are straight, but the faces of a hexahedron (trilinear image of a cube) need not be planar, and while the Jacobian of a bilinear mapping is linear, in general for a trilinear mapping it is nonlinear. The 2-D methods discussed here extend in one way or another to 3-D, and are in various stages of development for 3-D. However, for our introductory purposes here, we find it best to emphasize 2-D. For similar reasons, we consider only a linear pressure equation, and our focus is on logically rectangular meshes, though more complicated PDEs and grids of more general connectivity could be addressed.

Section 2 describes the lowest-order Raviart-Thomas (RT_0) [11, 12] mixed finite element (MFE) method, as a starting point to which other methods can be related. The analogous control-volume mixed (CVMFE) method [5] is introduced in Section 3, along with some modifications by Garanzha and Konshin [7] and some observations in [7] that relate the CVMFE to the support-operators (SO) method of Shashkov and co-workers [8, 10]. These methods are related in a different way in Section 4 to the multi-point flux approximation (MPFA) methods of Aavatsmark and co-workers [1, 2]. Section 4 also briefly discusses the expanded mixed (EM) method of Arbogast *et al.* [3, 4] and the mixed finite volume (MFV) method of Thomas and Trujillo [13], and Section 5 summarizes the paper.

2 RT_0 Mixed Method

A MFE represents a partial differential equation as a system of lower-order equations, solving these for multiple variables of physical interest. In the context of porous media, we assume incompressible flow, neglecting gravitational effects, so that the pressure equation (with no-flow boundary condition for simplicity) takes the form

$$-\nabla \cdot (\mathbf{K}\nabla p) = q, \qquad \mathbf{x} \in \Omega, \tag{2.1}$$

$$-\mathbf{K}\nabla p \cdot \mathbf{n} = 0, \qquad \mathbf{x} \in \partial\Omega, \tag{2.2}$$

where $\mathbf{K}$ (scalar or anisotropic tensor) is the mobility or hydraulic conductivity, p the pressure, q a source/sink (e.g., well) term, and Ω is the reservoir or aquifer with boundary $\partial\Omega$. Let $\mathbf{v}$ be the velocity vector, and express (2.1) as a system representing Darcy's law and conservation of mass, respectively:

$$\mathbf{v} = -\mathbf{K}\nabla p, \tag{2.3}$$

$$\nabla \cdot \mathbf{v} = q. \tag{2.4}$$

A primary goal is to obtain a more accurate $\mathbf{v}$, especially when $\mathbf{K}$ is heterogeneous, by solving the system (2.3)–(2.4) for $\mathbf{v}$ and p, instead of solving (2.1) for p and applying (2.3) to obtain $\mathbf{v}$. Piecewise-constant test functions in (2.7) below will also yield local mass conservation.

As in [11], let $\mathbf{V} = \{\mathbf{w} \in H(\mathrm{div}, \Omega) : \mathbf{w} \cdot \mathbf{n} = 0 \text{ on } \partial\Omega\}$, $P = L^2(\Omega)$, write (2.3) as

$$\mathbf{K}^{-1}\mathbf{v} + \nabla p = 0, \tag{2.5}$$

and arrive at the weak form of (2.3)–(2.4), which is to find $\mathbf{v} \in \mathbf{V}$ and $p \in P$ such that

$$\int_\Omega \mathbf{K}^{-1}\mathbf{v} \cdot \mathbf{w}\, d\mathbf{x} - \int_\Omega \nabla \cdot \mathbf{w}\, p\, d\mathbf{x} = 0, \qquad \mathbf{w} \in \mathbf{V}, \tag{2.6}$$

$$\int_\Omega \nabla \cdot \mathbf{v}\, z\, d\mathbf{x} = \int_\Omega q z\, d\mathbf{x}, \qquad z \in P. \tag{2.7}$$

The rectangular RT_0 elements define discrete subspaces $\mathbf{V}_h$ and P_h with respect to a cartesian grid. P_h consists of the piecewise-constant functions. $\mathbf{V}_h$ can best be viewed by associating a degree of freedom with the flux (constant normal component times edge length $|E|$) on each inter-block edge E. A typical basis function has flux 1 on one edge (D in Figure 1) and 0 on all others, with the flux varying linearly in the direction of the velocity. For arbitrary quadrilateral grids, appropriate pressure and velocity spaces are defined via the Piola mapping [11, 12] (see Section 3.2).

3 CVMFE and K^{-1} Methods

In addition to the local mass conservation provided by (2.7), the CVMFE seeks a local discrete Darcy law, which an engineer could view as applying to a cell-sized "tank" with pressures imposed at the ends. In the MFE context, this is analogous to the formulation of control-volume finite element (CVFE) methods from Galerkin FE, hence the name. We describe the formulation first on rectangles, then on distorted quadrilaterals.

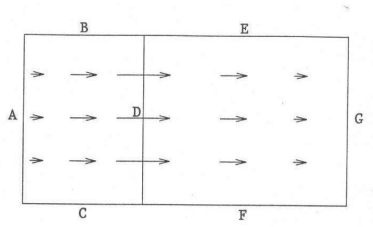

FIG. 1. RT_0 velocity basis function on rectangles.

3.1 Rectangular grid

Starting from the system (2.4)–(2.5), consider the pressure cells $Q_{i,j}$ and the control volumes $Q_{i+1/2,j}$ and $Q_{i,j+1/2}$ associated with the edge fluxes $(f_x)_{i+1/2,j}$ and $(f_y)_{i,j+1/2}$, as depicted in Figure 2. For this case, we take $\mathbf{K} = k$ to be scalar. The unknowns are associated with cells and edges as in the MFE, and the trial functions for $\mathbf{v}$ and p are again the RT_0 spaces. In the MFE, the test functions $\mathbf{w}$ and z are from the same spaces; in the CVMFE, (2.4) is still treated in this way, but the x- and y-components of the vector Darcy law (2.5) are instead integrated over "tanks" $Q_{i+1/2,j}$ and $Q_{i,j+1/2}$, respectively. This is equivalent to taking the scalar product of (2.5) with $\mathbf{w} = (1,0)$ on $Q_{i+1/2,j}$ and (0,0) elsewhere, and with $\mathbf{w} = (0,1)$ on $Q_{i,j+1/2}$ and (0,0) elsewhere, respectively, and integrating. The resulting partial derivatives of p can be integrated out, leaving

$$\int_{x_i}^{x_{i+1}} \int_{y_{j-1/2}}^{y_{j+1/2}} k^{-1} v_x(x,y)\, dy\, dx + \int_{y_{j-1/2}}^{y_{j+1/2}} (p(x_{i+1},y) - p(x_i,y))\, dy = 0, \quad (3.1)$$

and similarly for the y-component. Using the RT_0 trial functions, the integrals such as (3.1) are expressed in terms of the unknowns p, f_x, and f_y. We then obtain the discrete Darcy equations on the "tanks": in the x-direction on $Q_{i+1/2,j}$,

$$\begin{aligned} a_{i+1/2,j;A}(f_x)_{i-1/2,j} + a_{i+1/2,j;D}(f_x)_{i+1/2,j} & \\ + a_{i+1/2,j;G}(f_x)_{i+3/2,j} + p_{i+1,j} - p_{i,j} &= 0, \end{aligned} \quad (3.2)$$

where A, D, G refer to edges as in Figure 1, and

$$a_{i+1/2,j;A} = \frac{1}{8} \frac{k_{i,j}^{-1}}{|Q_{i,j}|} (\Delta x_i)^2, \quad (3.3)$$

$$a_{i+1/2,j;D} = \frac{3}{8} \frac{k_{i,j}^{-1}}{|Q_{i,j}|} (\Delta x_i)^2 + \frac{3}{8} \frac{k_{i+1,j}^{-1}}{|Q_{i+1,j}|} (\Delta x_{i+1})^2, \quad (3.4)$$

$$a_{i+1/2,j;G} = \frac{1}{8}\frac{k_{i+1,j}^{-1}}{|Q_{i+1,j}|}(\Delta x_{i+1})^2, \tag{3.5}$$

where $\Delta x_i = x_{i+1/2} - x_{i-1/2}$, $\Delta x_{i+1} = x_{i+3/2} - x_{i+1/2}$, with an analogous equation in the y-direction on $Q_{i,j+1/2}$.

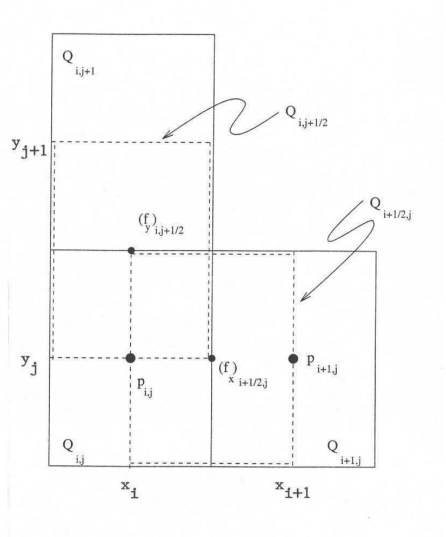

FIG. 2. Cells, unknowns, and control volumes for rectangular grid.

Integration of (2.4) over the cell $Q_{i,j}$ (equivalent to multiplying by a test function $z = 1$ on $Q_{i,j}$ and 0 elsewhere), together with the Gauss divergence theorem, yields the discrete mass conservation:

$$(f_x)_{i-1/2,j} - (f_x)_{i+1/2,j} + (f_y)_{i,j-1/2} - (f_y)_{i,j+1/2} = -|Q_{i,j}|q_{i,j}. \tag{3.6}$$

Equation (3.2), its y-analogue, and (3.6) give rise to a symmetric system of linear equations that is solved for the pressures at block centers and the fluxes across edges.

3.2 Distorted quadrilateral grid

If Q is a convex quadrilateral, then there is a unique bilinear mapping of a reference square $\hat{Q} = [0,1]^2$ onto Q that sets up coordinates on Q. The pressure in Q is associated with the "center" of Q, meaning the image of the center of $\hat{Q}$. Note that this is not generally the centroid of Q.

The extension of the CVMFE method to general quadrilaterals requires that continuity of flux be maintained, so that the normal component of a

velocity function must be constant on each edge. Then we can associate degrees of freedom with fluxes on edges, as in the rectangular case. In Figure 3 we show two adjacent quadrilaterals with coordinates determined by their local bilinear mappings. The velocity vector function $\mathbf{v}_{i+1/2,j}$ that has flux 1 (hence normal component $1/|E_{i+1/2,j}|$) on the common edge $E_{i+1/2,j}$ (labeled in Figure 4) and 0 on the other edges is pictured. It is oriented along x-coordinate lines, and has constant normal component on each complementary y-line, with the flux varying linearly in the x-direction.

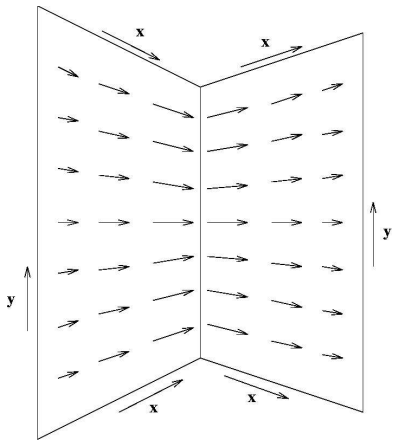

FIG. 3. Velocity basis function $\mathbf{v}_{i+1/2,j}$ on quadrilaterals.

Let $\hat{x}, \hat{y} \in [0,1]$ be the reference coordinates for a quadrilateral Q. Set

$$\mathbf{X}(\hat{x},\hat{y}) = \left(\frac{\partial x}{\partial \hat{x}}, \frac{\partial y}{\partial \hat{x}}\right) \tag{3.7}$$

$$\mathbf{Y}(\hat{x},\hat{y}) = \left(\frac{\partial x}{\partial \hat{y}}, \frac{\partial y}{\partial \hat{y}}\right) \tag{3.8}$$

to be the columns of the Jacobian matrix of the bilinear mapping. These can be viewed as the images of the vectors $(1,0)$ and $(0,1)$, respectively, under the mapping from $\hat{Q}$ to Q. For example, the $\mathbf{v}_{i+1/2,j}$ in Figure 3 is parallel to $\mathbf{X}$, and after some manipulation, one can show that it is given on the left-hand quadrilateral $Q_{i,j}$ by

$$\mathbf{v}_{i+1/2,j}(x,y) = \frac{\hat{x}\mathbf{X}}{J_{i,j}(\hat{x},\hat{y})}, \tag{3.9}$$

where

$$J_{i,j}(\hat{x},\hat{y}) = \frac{\partial x}{\partial \hat{x}}\frac{\partial y}{\partial \hat{y}} - \frac{\partial x}{\partial \hat{y}}\frac{\partial y}{\partial \hat{x}} \tag{3.10}$$

is the Jacobian of the mapping from $\hat{Q}$ to $Q_{i,j}$. In the right-hand quadrilateral $Q_{i+1,j}$, everything is the same except that $1-\hat{x}$ and $J_{i+1,j}$ replace $\hat{x}$ and $J_{i,j}$, respectively. These velocity trial functions and unknowns (fluxes across edges) can also be obtained from those on rectangles by a Piola transformation [12]. Define also the corresponding unit normal vectors, $\mathbf{n}_x \perp \mathbf{Y}$, $\mathbf{n}_y \perp \mathbf{X}$, pictured in Figure 4:

$$\mathbf{n}_x = \frac{(\partial y/\partial\hat{y}, -\partial x/\partial\hat{y})}{[(\partial x/\partial\hat{y})^2 + (\partial y/\partial\hat{y})^2]^{1/2}}, \tag{3.11}$$

$$\mathbf{n}_y = \frac{(-\partial y/\partial\hat{x}, \partial x/\partial\hat{x})}{[(\partial x/\partial\hat{x})^2 + (\partial y/\partial\hat{x})^2]^{1/2}}. \tag{3.12}$$

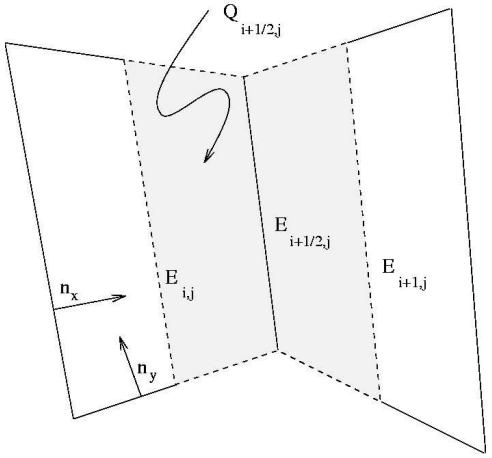

FIG. 4. Control-volume mixed finite elements on quadrilaterals.

It remains to choose control volumes and test functions. For the integrations of (2.4), the control volumes are the quadrilateral blocks $Q_{i,j}$, and the test functions are scalar characteristic functions of the control volumes, i.e., functions that are 1 on one volume and zero elsewhere. The Gauss divergence theorem then yields (3.6) for quadrilaterals as well as rectangles.

For the integrations of (2.5), to mimic the steps leading to (3.1), we use images of rectangular control volumes $Q_{i+1/2,j}$ and $Q_{i,j+1/2}$ under the bilinear mapping, as seen in Figure 4. We again denote such control volumes by $Q_{i+1/2,j}$ and $Q_{i,j+1/2}$. $Q_{i+1/2,j}$ in Figure 4 will be the "tank" with pressures $p_{i,j}$ and $p_{i+1,j}$ at the two ends. We seek test functions that allow the gradient of p to be integrated out, leaving differences of p.

Let $Q_{i+1/4,j}$ and $Q_{i+3/4,j}$ denote the "left-hand half" and "right-hand half," respectively, of $Q_{i+1/2,j}$. Then $Q_{i+1/4,j}$ is the image of the right-hand

half, $(1/2,1)\times(0,1)$, of $\hat{Q}$ under the mapping to $Q_{i,j}$. The original CVMFE [5] used $\mathbf{X}$ as the test function, which led to integrals that could be calculated analytically, with a factor of $1/J$ outside the integral; the modification suggested by Garanzha and Konshin [7] instead uses $\mathbf{X}/J$, which requires numerical integration but gains accuracy on highly distorted meshes. By their approach, the left-half p integral analogous to the one in (3.1) is

$$\begin{aligned}\int_{Q_{i+1/4,j}} \nabla p\cdot(\mathbf{X}_{i,j}/J_{i,j})\,d\mathbf{x} &= \int_0^1\int_{1/2}^1 \frac{\partial p}{\partial\hat{x}}\,d\hat{x}\,d\hat{y}\\ &= \int_0^1 p(1,\hat{y})\,d\hat{y} - \int_0^1 p(1/2,\hat{y})\,d\hat{y}\\ &\approx p_{i+1/2,j} - p_{i,j}, \end{aligned}\tag{3.13}$$

where the last step involves p at edge and cell centers and is exact for bilinear p. In defining the CVMFE equations, treat (3.13) as exact, i.e., ignore truncation error. Similarly, the right-half integral yields

$$\int_{Q_{i+3/4,j}} \nabla p\cdot(\mathbf{X}_{i+1,j}/J_{i+1,j})\,d\mathbf{x} = p_{i+1,j} - p_{i+1/2,j}. \tag{3.14}$$

Hence, by choosing the test vector field

$$\mathbf{w}_{i+1/2,j} = \begin{cases} \mathbf{X}_{i,j}/J_{i,j} & \text{on } Q_{i+1/4,j},\\ \mathbf{X}_{i+1,j}/J_{i+1,j} & \text{on } Q_{i+3/4,j},\\ \mathbf{0} & \text{elsewhere,}\end{cases} \tag{3.15}$$

we combine (3.13)–(3.14) into

$$\int_{Q_{i+1/2,j}} \nabla p\cdot\mathbf{w}_{i+1/2,j}\,d\mathbf{x} = p_{i+1,j} - p_{i,j}, \tag{3.16}$$

and the edge value $p_{i+1/2,j}$ is eliminated. If desired, it can be recovered later in a postprocessing step.

With the test function from (3.15), the $\mathbf{v}$ term of (2.5) can be calculated as in [5], leading to the discrete Darcy equation analogous to (3.2), with edges denoted as in Figure 1:

$$\begin{aligned} a_{i+1/2,j;A}(f_x)_{i-1/2,j} + a_{i+1/2,j;D}(f_x)_{i+1/2,j} + a_{i+1/2,j;G}(f_x)_{i+3/2,j}\\ +a_{i+1/2,j;B}(f_y)_{i,j+1/2} + a_{i+1/2,j;C}(f_y)_{i,j-1/2}\\ +a_{i+1/2,j;E}(f_y)_{i+1,j+1/2} + a_{i+1/2,j;G}(f_y)_{i+1,j-1/2}\\ +p_{i+1,j} - p_{i,j} = 0, \end{aligned}\tag{3.17}$$

where the coefficients in (3.17) are given by

$$a_{i+1/2,j;D} = \int_0^1 \int_{1/2}^1 \hat{x}(\mathbf{K}_{i,j}^{-1}\mathbf{X}_{i,j}) \cdot \mathbf{X}_{i,j}/J_{i,j}\, d\hat{x}\, d\hat{y} \qquad (3.18)$$
$$\int_0^1 \int_0^{1/2} (1-\hat{x})(\mathbf{K}_{i+1,j}^{-1}\mathbf{X}_{i+1,j}) \cdot \mathbf{X}_{i+1,j}/J_{i+1,j}\, d\hat{x}\, d\hat{y},$$

$$a_{i+1/2,j;A} = \int_0^1 \int_{1/2}^1 (1-\hat{x})(\mathbf{K}_{i,j}^{-1}\mathbf{X}_{i,j}) \cdot \mathbf{X}_{i,j}/J_{i,j}\, d\hat{x}\, d\hat{y}, \qquad (3.19)$$

$$a_{i+1/2,j;G} = \int_0^1 \int_0^{1/2} \hat{x}(\mathbf{K}_{i+1,j}^{-1}\mathbf{X}_{i+1,j}) \cdot \mathbf{X}_{i+1,j}/J_{i+1,j}\, d\hat{x}\, d\hat{y}, \qquad (3.20)$$

$$a_{i+1/2,j;B} = \int_0^1 \int_{1/2}^1 \hat{y}(\mathbf{K}_{i,j}^{-1}\mathbf{Y}_{i,j}) \cdot \mathbf{X}_{i,j}/J_{i,j}\, d\hat{x}\, d\hat{y}, \qquad (3.21)$$

$$a_{i+1/2,j;C} = \int_0^1 \int_{1/2}^1 (1-\hat{y})(\mathbf{K}_{i,j}^{-1}\mathbf{Y}_{i,j}) \cdot \mathbf{X}_{i,j}/J_{i,j}\, d\hat{x}\, d\hat{y}, \qquad (3.22)$$

$$a_{i+1/2,j;E} = \int_0^1 \int_0^{1/2} \hat{y}(\mathbf{K}_{i+1,j}^{-1}\mathbf{Y}_{i+1,j}) \cdot \mathbf{X}_{i+1,j}/J_{i+1,j}\, d\hat{x}\, d\hat{y}, \qquad (3.23)$$

$$a_{i+1/2,j;F} = \int_0^1 \int_0^{1/2} (1-\hat{y})(\mathbf{K}_{i+1,j}^{-1}\mathbf{Y}_{i+1,j}) \cdot \mathbf{X}_{i+1,j}/J_{i+1,j}\, d\hat{x}\, d\hat{y}. \qquad (3.24)$$

The Darcy equation for the horizontal edge $E_{i,j+1/2}$ is analogous, with the roles of the x- and y-directions reversed. That equation, with (3.6) and (3.17), forms the discrete system for CVMFE.

As the trial and test functions are different for CVMFE, the discrete equations may not be symmetric. A representative example is (3.21), in which test function $\mathbf{w}_{i+1/2,j}$ interacts with trial function $\mathbf{v}_{i,j+1/2}$. Symmetry would require that (3.21) yield the same result as

$$a_{i,j+1/2;B} = \int_{1/2}^1 \int_0^1 \hat{x}(\mathbf{K}_{i,j}^{-1}\mathbf{X}_{i,j}) \cdot \mathbf{Y}_{i,j}/J_{i,j}\, d\hat{x}\, d\hat{y}. \qquad (3.25)$$

Since (3.21) and (3.25) integrate over different (but overlapping) half-cells, symmetry cannot hold in general with variable J (with constant J, $\mathbf{X}$, $\mathbf{Y}$, as on a grid of parallelograms, symmetry does hold). However, with a quadrature rule that receives no contribution from the nonoverlapping parts of the half-cells, i.e., one whose nonoverlapping points have $\hat{y} = 0$ in (3.21) and $\hat{x} = 0$ in (3.25), symmetry is possible. As noted by Garanzha and Konshin

[7], for the half-cell in (3.21), a rule of the form

$$\begin{aligned}\int_0^1 \int_{1/2}^1 g\, d\hat{x}\, d\hat{y} &\approx r(g(1/2,0) + 2g(1,1/2) + g(1/2,1)) \\ &+ (1/8 - r)(g(1,0) + 2g(1/2,1/2) + g(1,1)), \quad (3.26)\end{aligned}$$

where $0 \le r \le 1/8$, preserves symmetry and also integrates bilinear g exactly. With such a quadrature, the entire discrete system is symmetric, and for parallelograms all integrals are exact; in particular, the weights $1/8, 6/8, 1/8$ in (3.3)–(3.5) are preserved. We note here that the corresponding weights for MFE are $1/6, 4/6, 1/6$, and that MFE is symmetric with any consistent quadrature because the trial and test functions coincide. Because the MFE integrands that produce these weights are quadratic, it is possible within the MFE framework, with a rule that is not exact for quadratics, to produce the CVMFE weights and the CVMFE formulas resulting from quadrature rule (3.26) [7]. In general, it is not possible to produce the exact CVMFE formulas in this way, as they are nonsymmetric.

Quadrature provides a convenient framework within which to consider the technique of mass lumping, which is often used to simplify finite element methods, producing a diagonal mass matrix and reducibility to finite differences. In the context of CVMFE equations (3.18)–(3.24), this is equivalent to setting $\hat{x}$, $1 - \hat{x}$, $\hat{y}$, and $1 - \hat{y}$ equal to 1 whenever they are greater than $1/2$, and 0 otherwise, then integrating. In (3.26), this would correspond to a quadrature with $\hat{x} = 1$ and $\hat{y} = 0$ or 1, i.e.,

$$\int_0^1 \int_{1/2}^1 g\, d\hat{x}\, d\hat{y} \approx 1/4\,(g(1,0) + g(1,1)). \quad (3.27)$$

This quadrature preserves symmetry, just as (3.26) does, but it does not integrate bilinear g exactly; indeed, it must not, because it changes the weights $1/8, 6/8, 1/8$ in (3.3)–(3.5) to $0, 1, 0$. Garanzha and Konshin [7] (p. 24) note that this lumping produces the SO method [8, 10]. Thus, CVMFE and SO are related in much the same way as CVFE and conventional point-centered finite differences.

4 Relationships to K Methods

In the petroleum industry, there is considerable recent work [1, 2, 6, 9] on discretizations that take a view dual to that of formulas such as (3.17). We

call the methods of Section 3 "$\mathbf{K}^{-1}$ methods" because, when complicated details are ignored, they reduce to a relationship of the form

$$-\mathbf{K}^{-1}\,\mathbf{f} = \Delta p, \tag{4.1}$$

where $\mathbf{f}$ is the flux vector and Δp the pressure difference. $\mathbf{K}^{-1}$ appears discretely as a mass matrix, so that a combination of fluxes equals a pressure drop. "$\mathbf{K}$ methods," on the other hand, adopt the perspective that

$$\mathbf{f} = -\mathbf{K}\,\Delta p, \tag{4.2}$$

expressing an individual discrete flux as a combination of pressure drops. As a prototype of these methods, we consider the MPFA scheme of Aavatsmark *et al.* [1, 2] and seek to relate $\mathbf{K}^{-1}$ methods to it. It seems natural to attempt to pass from (4.1) to (4.2) by inverting $\mathbf{K}^{-1}$. To avoid a full stencil in (4.2) even for orthogonal grids, it is necessary to lump the principal weights in $\mathbf{K}^{-1}$, such as the $1/8, 6/8, 1/8$ for CVMFE. For the contributions to $\mathbf{K}^{-1}$ caused by non-orthogonality and/or anisotropy, some form of incomplete inversion is suggested.

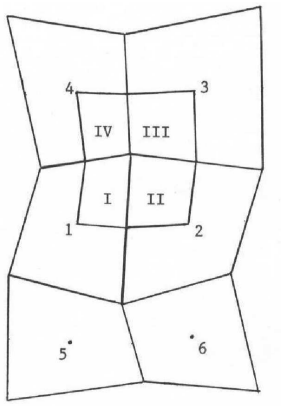

FIG. 5. Cells and interaction region for MPFA method.

To describe the MPFA method, we refer to Figure 5. The pressure p is to be determined at the cell centers and is assumed to be linear (not bilinear) on each piece I,II,III,IV of the interaction region. Thus, there are 12 degrees of freedom on that region, and 12 constraints are imposed: 4 cell-center values, continuity of p at the 4 points where the interaction-region boundary crosses a cell edge, and continuity of the flux across the 4 interfaces in the region.

To close this system, the relation

$$f_E = -\int_E \mathbf{K}\nabla p \cdot \mathbf{n}\, dS \tag{4.3}$$

between the pressure and the fluxes across edges is needed. With a bilinear reference mapping to a distorted quadrilateral, as in Section 3, this can be written

$$\begin{aligned} f_x &= a\frac{\partial p}{\partial \hat{x}} + c\frac{\partial p}{\partial \hat{y}}, \\ f_y &= c\frac{\partial p}{\partial \hat{x}} + b\frac{\partial p}{\partial \hat{y}}, \end{aligned} \tag{4.4}$$

where

$$\begin{aligned} a &= -J\,(\mathbf{K}\nabla\hat{x})\cdot\nabla\hat{x} = -(\mathbf{Y}\cdot\mathbf{Y}/J)\,(\mathbf{K}\mathbf{n}_x)\cdot\mathbf{n}_x, \\ b &= -J\,(\mathbf{K}\nabla\hat{y})\cdot\nabla\hat{y} = -(\mathbf{X}\cdot\mathbf{X}/J)\,(\mathbf{K}\mathbf{n}_y)\cdot\mathbf{n}_y, \\ c &= -J\,(\mathbf{K}\nabla\hat{x})\cdot\nabla\hat{y} = -(|\mathbf{X}||\mathbf{Y}|/J)\,(\mathbf{K}\mathbf{n}_x)\cdot\mathbf{n}_y. \end{aligned} \tag{4.5}$$

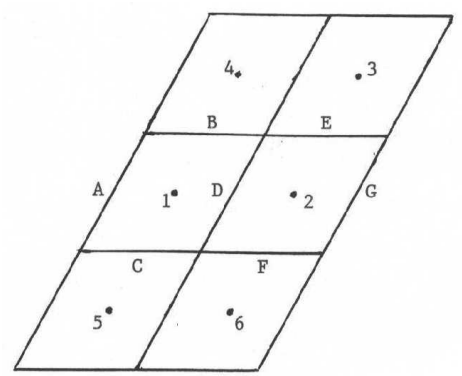

FIG. 6. Uniform grid of parallograms.

This is best understood in a simple case, where a, b, c are constants. In Figure 6 we show a grid of parallelograms that meets this criterion, since J, $\mathbf{X}$, $\mathbf{Y}$ are constants, and assume also that $\mathbf{K} = k$ is a scalar constant. Referring to Figure 6, solution of the 12 equations leads to [1]

$$f_D = \left(a - \frac{c^2}{2b}\right)(p_2 - p_1) + \frac{c}{4}\left(1 + \frac{c}{b}\right)(p_3 - p_5) + \frac{c}{4}\left(1 - \frac{c}{b}\right)(p_4 - p_6). \tag{4.6}$$

(For no distortion, $c = 0$, and (4.6) reduces to $f_D = a(p_2 - p_1)$, as expected for finite differences.) If θ is the angle of distortion ($\theta = 0$ for rectangles,

$\mathbf{X}\cdot\mathbf{Y} = |\mathbf{X}||\mathbf{Y}|\sin\theta$), then $J = |\mathbf{X}||\mathbf{Y}|\cos\theta$, $\mathbf{n}_x\cdot\mathbf{n}_y = -\sin\theta$, and

$$a = \frac{-Jk}{\mathbf{X}\cdot\mathbf{X}\cos^2\theta}, \qquad b = \frac{-Jk}{\mathbf{Y}\cdot\mathbf{Y}\cos^2\theta}, \qquad c = k\tan\theta = k\,\frac{\mathbf{X}\cdot\mathbf{Y}}{J}, \quad (4.7)$$

whence

$$a - \frac{c^2}{2b} = -\frac{Jk}{\mathbf{X}\cdot\mathbf{X}}, \qquad \frac{c}{4} = \frac{1}{4}\,k\frac{\mathbf{X}\cdot\mathbf{Y}}{J}. \quad (4.8)$$

Next, we evaluate the coefficients in the $\mathbf{K}^{-1}$ methods. For the configuration in Figure 6, we write the analogue of (3.17),

$$a_A f_A + a_B f_B + a_C f_C + a_D f_D + a_E f_E + a_F f_F + a_G f_G + p_2 - p_1 = 0, \quad (4.9)$$

where, by (3.18)–(3.24),

$$\begin{aligned} a_D &= \frac{6}{8}\,\frac{k^{-1}\mathbf{X}\cdot\mathbf{X}}{J}, \qquad a_A = a_G = \frac{1}{8}\,\frac{k^{-1}\mathbf{X}\cdot\mathbf{X}}{J}, \\ & a_B = a_C = a_E = a_F = \frac{1}{4}\,\frac{k^{-1}\mathbf{Y}\cdot\mathbf{X}}{J}. \end{aligned} \quad (4.10)$$

For MFE, the coefficients $6/8, 1/8$ in (4.10) become $4/6, 1/6$; for lumping (SO), they are $1, 0$; for all of the $\mathbf{K}^{-1}$ methods, the $1/4$ holds. As noted above, before inverting $\mathbf{K}^{-1}$, it is best to lump; doing so, and using (4.8),

$$\begin{aligned} p_2 - p_1 &= -\frac{k^{-1}\mathbf{X}\cdot\mathbf{X}}{J}(f_D + \epsilon(f_B + f_C + f_E + f_F)), \\ &= \left(a - \frac{c^2}{2b}\right)^{-1}((\mathbf{I} + \epsilon\mathbf{N})f)_D, \end{aligned} \quad (4.11)$$

where

$$\epsilon = \frac{1}{4}\frac{\mathbf{X}\cdot\mathbf{Y}}{\mathbf{X}\cdot\mathbf{X}} \quad (4.12)$$

and $\mathbf{N}$ is a matrix with 1's on 4 off-diagonals. Now, because

$$(\mathbf{I} + \epsilon\mathbf{N})^{-1} = \mathbf{I} - \epsilon\mathbf{N} + O(\epsilon^2), \quad (4.13)$$

we can perform an incomplete inversion and write

$$f_D = \left(a - \frac{c^2}{2b}\right)(p_2 - p_1 - \epsilon[(p_4 - p_1) + (p_3 - p_2) + (p_1 - p_5) + (p_2 - p_6)]). \quad (4.14)$$

The leading terms of (4.6) and (4.14) match. The terms of first order in c would match if

$$c = -4\epsilon\left(a - \frac{c^2}{2b}\right). \quad (4.15)$$

A calculation from (4.8) and (4.12) shows that actually

$$c = -4\epsilon \left(a - \frac{c^2}{2b} \right) \left(\frac{\mathbf{X} \cdot \mathbf{X}}{J} \right)^2 . \tag{4.16}$$

Thus, it could be of interest to study how these methods relate on significantly distorted grids with large aspect ratios.

Arbogast *et al.* [3, 4] and Thomas and Trujillo [13] have developed other distorted-grid $\mathbf{K}$ methods derived from MFE formulations. The complexities are such that we can only give sketchy qualitative descriptions here. The expanded mixed (EM) method circumvents the difficulty of inverting $\mathbf{K}^{-1}$ by introducing an additional auxiliary variable, $\tilde{\mathbf{v}} = -\nabla p$, and then incorporating the relation $\mathbf{v} = \mathbf{K}\tilde{\mathbf{v}}$ into the weak form. The usual MFE for div ($\mathbf{K}$ grad), if reduced to a single equation for the pressure, leads to a discrete matrix $\mathbf{N}^T\mathbf{M}^{-1}\mathbf{N}$, where the three factors essentially discretize div, $\mathbf{K}$, and grad, respectively; $\mathbf{M}$ is sparse, but $\mathbf{M}^{-1}$ is full. The EM puts $\mathbf{K}$ on the right-hand side of the system, where its connectivity is sparse, in place of $\mathbf{K}^{-1}$ on the left. Low-order integration (midpoint and trapezoidal rules) leads to lumping and a compact stencil (9-point in 2-D, 19-point in 3-D) for use in finite difference codes. It seems likely that this scheme is related to lumped incompletely inverted $\mathbf{K}^{-1}$ methods, because such methods can obtain the same stencils in 2-D and 3-D, but this is speculative at this point. The method also uses Lagrange multipliers, representing edge pressures, where the grid is not smooth; another speculation is that these are related to the CVMFE edge pressure values that were eliminated in (3.16). The aim of Thomas and Trujillo is a MFV formulation that admits both a discrete pressure and a discrete velocity that have the regularity of their physical counterparts, i.e., $p \in H^1(\Omega)$ and $\mathbf{v} \in H(\mathrm{div}, \Omega)$. In the usual MFE approaches, $\mathbf{v}$ satisfies this criterion, but p does not. The discrete MFV pressure is continuous piecewise bilinear on a primal grid, with test functions that are constant on dual cells centered around the vertices of the primal cells. The trial and test functions for $\mathbf{v}$ are similar to those for the CVMFE method, but on a finer mesh. This appears to be substantially different from all of the other methods discussed here.

5 Summary

The challenge of constructing accurate discretization methods for heterogeneous, anisotropic problems on distorted grids has given rise to a wide variety

of approaches. The ones considered here (MFE, CVMFE, SO, MPFA, EM, MFV) share the property of conserving mass locally on discrete cells. Thus, in some sense they are all finite-volume methods. Broadly, they can be categorized as $\mathbf{K}$ or $\mathbf{K}^{-1}$ methods, depending on which way they formulate the conductivity coefficient. Typically a $\mathbf{K}$ method relates a flux to a combination of pressure differences, while a $\mathbf{K}^{-1}$ method relates a pressure difference to a combination of fluxes. Cell-centered finite difference and mixed finite element methods are standard representatives of these respective groups. Quadrature, mass lumping, and incomplete inversion of the mass matrix appear to be the concepts that can illuminate the interconnections between various schemes. Further study of these issues, particularly in 3-D, should be of significant benefit for practical modeling of flow in porous media.

Acknowledgments. This research was supported in part by National Science Foundation Grant No. DMS-9706866 and Army Research Office Grant No. 37119-GS-AAS.

References

[1] Aavatsmark, I., Barkve, T., Bøe, Ø., and Mannseth, T., Discretization on non-orthogonal, quadrilateral grids for inhomogeneous, anisotropic media, *J. Comp. Phys.* **127** (1996), 2–14.

[2] Aavatsmark, I., Barkve, T., and Mannseth, T., Control-volume discretization methods for 3D quadrilateral grids in inhomogeneous, anisotropic reservoirs, *Soc. Pet. Eng. J.* **3** (1998), 146–154.

[3] Arbogast, T., Keenan, P., Wheeler, M., and Yotov, I., Logically rectangular mixed methods for Darcy flow on general geometry, *Proc. 13th SPE Symposium on Reservoir Simulation*, Society of Petroleum Engineers, Dallas, 1995, pp. 51–59.

[4] Arbogast, T., Wheeler, M. F., and Yotov, I., Mixed finite elements for elliptic problems with tensor coefficients as cell-centered finite differences, *SIAM J. Numer. Anal.* **34** (1997), 828–852.

[5] Cai, Z., Jones, J. E., McCormick, S. F., and Russell, T. F., Control-volume mixed finite element methods, *Computational Geosciences* **1** (1997), 289–315.

[6] Edwards, M. G., Cross-flow, tensors and finite volume approximation with deferred correction, *Comp. Meth. Appl. Mech. Engrg.* **151** (1998), 143–161.

[7] Garanzha, V. A., and Konshin, V. N., Approximation schemes and discrete well models for the numerical simulation of the 2-D non-Darcy fluid flows in porous media, *Comm. on Appl. Math.*, Computer Centre, Russian Academy of Sciences, Moscow, 1999.

[8] Hyman, J., Shashkov, M., and Steinberg, S., The numerical solution of diffusion problems in strongly heterogeneous non-isotropic materials, *J. Comp. Phys.* **132** (1997), 130–148.

[9] Lee, S. H., Tchelepi, H., and DeChant, L. F., Implementation of a flux-continuous finite difference method for stratigraphic, hexahedron grids, *Proc. 15th SPE Symposium on Reservoir Simulation*, Society of Petroleum Engineers, Dallas, 1999, pp. 231–241.

[10] Morel, J. E., Hall, M. L., and Shashkov, M. J., A local support-operators diffusion discretization scheme for hexahedral meshes, Report LA-UR-99-4358, Los Alamos National Laboratory, 1999.

[11] Raviart, P. A., and Thomas, J.-M., A mixed finite element method for 2nd order elliptic problems, *Mathematical Aspects of Finite Element Methods*, I. Galligani and E. Magenes, ed., Springer-Verlag, 1977, pp. 292–315.

[12] Thomas, J.-M., *Sur l'analyse numérique des méthodes d'éléments finis hybrides et mixtes*, Ph.D. Thesis, Université Pierre et Marie Curie, 1977.

[13] Thomas, J.-M., and Trujillo, D., Analysis of finite volume methods, *Mathematical Modelling of Flow Through Porous Media*, A. Bourgeat *et al.*, ed., World Scientific, Singapore, 1995, pp. 318–336.

Thomas F. Russell
Department of Mathematics
University of Colorado at Denver
P.O. Box 173364, Campus Box 170
Denver, CO 80217-3364, U.S.A.
thomas.russell@cudenver.edu